Transport properties of n- and p-type polycrystalline BaSi2

doi: 10.1016/j.tsf.2018.07.006

Transport properties of n- and p-type polycrystalline $BaSi_2$

T. Deng and T. Suemasu

Institute of Applied Physics, University of Tsukuba, Tsukuba, Ibaraki 305-8573, Japan

suemasu@bk.tsukuba.ac.jp

D. A. Shohonov, I. S. Samusevich, A. B. Filonov, D. B. Migas, and V. E. Borisenko

Department of Micro- and Nanoelectronics,

Belarusian State University of Informatics and Radioelectronics,

P. Browki 6, 220013 Minsk, Belarus

migas@bsuir.by

Electron and hole mobilities versus temperature in semiconducting barium disilicide ($BaSi_2$) have been systematically studied both experimentally and theoretically. The experiments were performed with undoped 250 nm-thick $BaSi_2$ polycrystalline films grown by molecular beam epitaxy. The grain size of films ranged from 0.2 to 5 μm with the electron concentration of 5.0×10^{15} cm^{-3}. To investigate the hole mobility, B-doped *p*-$BaSi_2$ films with various dopant concentrations were fabricated and studied. The experimental temperature dependence of the electron mobility in the range of 160 – 300 K was found to have a maximum of 1230 $cm^2/V{\cdot}s$ at 218 K, while at room temperature (RT) it dropped down to 816 $cm^2/V{\cdot}s$. We demonstrate that the temperature dependence of the electron mobility cannot be adequately reproduced by involving standard scattering mechanisms. A modified approach accounting for the grained nature of the films has been proposed for the correct description of the mobility behavior. The highest hole mobility in *p*-$BaSi_2$ films reaching ~ 80 or 200 $cm^2/V{\cdot}s$ (for the films grown on (111) or (001) Si substrates, respectively) at RT is about an order or four times of magnitude smaller than that in *n*-$BaSi_2$ films. Such a great difference we ascribe to the specific features of electron-phonon and hole-phonon coupling in semiconducting $BaSi_2$.

Keywords: Barium disilicide, polycrystalline film, Hall measurement, electron and hole mobilities.

1. Introduction

Nowadays efficient solar energy conversion is a very challenging task because it requires semiconducting materials with appropriate optical and carrier transport properties to effectively absorb solar light for electron-hole pair generation and to avoid the recombination of the pairs by spatial separation of electrons and holes [1]. Barium disilicide ($BaSi_2$), which is well compatible with the conventional silicon technology and an environmentally friendly material, possesses the band gap of 1.15 – 1.30 eV [2], the rather large optical absorption coefficient near the absorption edge and the large minority-carrier diffusion length in addition to the long minority-carrier lifetime [3]. Thus, it promises to be very efficient in solar cell applications [3]. Recently, we successfully fabricated B-doped *p*-$BaSi_2$/*n*-Si heterojunction solar cells on both Si (111) and Si (001) substates with efficiency approaching 10% [4, 5], and achieved the operation of $BaSi_2$ homojunction solar cells [6]. $BaSi_2$ is also attractive for thermoelectric applications because of the large value of the Seebeck coefficient [7]. There are some investigations devoted to the study of $BaSi_2$ basic electronic and optical properties [8, 9], but at the same time there is almost the lack of information on its transport properties. Here we present extended experimental data on the mobility of electrons and holes in $BaSi_2$ in the temperature range 50 – 300 K along with their theoretical interpretation.

2. Experimental

An ion-pumped molecular beam epitaxy (MBE) system equipped with standard Knudsen cells (K-cells) for Ba and B, and an electron-beam evaporation source for Si was applied. For the fabrication of undoped *n*-$BaSi_2$ films a silicon-on-insulator substrate with a 1 μm-thick *n*-Si(111) topmost layer (ρ > 1000 Ωcm) was used. This substrate was formed by bonding 500 μm-thick high-resistivity floating-zone (FZ) *n*-Si(111) and SiO_2-capped Si(001) handle wafers. Then, the FZ-Si wafer was mechanically ground and polished by chemical mechanical polishing down to about 1 μm thickness. On the other hand, for B-doped *p*-$BaSi_2$ films [10, 11], we used 500 μm-thick high-resistivity (ρ > 1000 Ωcm) FZ *n*-Si(111) and *n*-Si(001) substrates. For all the samples,

after cleaning the substrate by heating at 900 ºC for 30 min in ultrahigh vacuum, a 5 nm-thick $BaSi_2$ template layer was grown on the Si substrate synthesized by reactive deposition epitaxy (RDE) at 500 ºC using only the Ba source [12]. This template layer works as a kind of seed crystals for the subsequent $BaSi_2$ layer [13]. Then a 250 nm-thick undoped $BaSi_2$ film was formed on top of the template at 600 ºC in the MBE mode using both Ba and Si sources [14]. For B-doped *p*-$BaSi_2$ films, Ba, Si, and B were evaporated on the template layer at 600 ºC. The B concentration was controlled by the crucible temperature of the B K-cell (T_B) which was varied as 1000, 1100, 1170, 1230, and 1300 ºC. They are denoted as samples #1 – #5, respectively. Afterwards, a 3 nm-thick a-Si layer was deposited to prevent oxidation of the $BaSi_2$ films. The deposition rates of Si and Ba were controlled using an electron impact emission spectroscopy (EIES; INFICON) feedback system.

The crystal structure of the films was characterized by X-ray diffraction (XRD) using Cu Kα radiation and plan-view transmission electron microscopy (TEM) in TOPCON EM-002 device operated at 120 kV. Electron backscatter diffraction (EBSD) analyses were performed to analyze the grain size of $BaSi_2$. Concentration and mobility of electrons and holes, which were main charge carriers in the fabricated undoped and B-doped films, respectively, were measured by the Hall technique at temperatures between 20 and 300 K using a closed-cycle He cryostat on the van der Pauw structures with ohmic contacts made by sputtered Al. The applied magnetic field was 0.2 T. The measurement temperature was limited down to 145 K for undoped *n*-$BaSi_2$, because of the difficulty in assuring ohmic contacts at such low temperatures. The electron concentration (*n*) of undoped $BaSi_2$ extracted from the Hall measurements occurred to be 5.0×10^{15} cm^{-3} at room temperature (RT). This value has been cross-checked by another method using the slope of the $1/C^2$ versus voltage plot, where *C* is the capacitance [15]. The activation energy of donor levels was approximately 30 meV, and the electron concentration did not change a lot in the measurement temperature range of 150–300 K [14]. The hole concentration (*p*) of B-doped *p*-$BaSi_2$ on Si(111) also did not show any significant change in the measurement

temperature range of 50–300 K, but depended on T_B thereby the B concentration and it was varied from 5.0×10^{16} to 5.3×10^{18} cm^{-3} at RT. The activation energy of acceptor levels was in the range between 20 and 30 meV [10]. The fact that the $BaSi_2$ is a semiconducting material in the above temperature range has been confirmed by the temperature dependence of spectral response [15]. B concentration (N_B) was determined by secondary ion mass spectrometry (SIMS) using C_S ions. Figure 1 shows Arrhenius plots of N_B in B-doped $BaSi_2$ films. SIMS measurements revealed that as T_B increases, N_B increases exponentially with an activation energy of 6.2 eV.

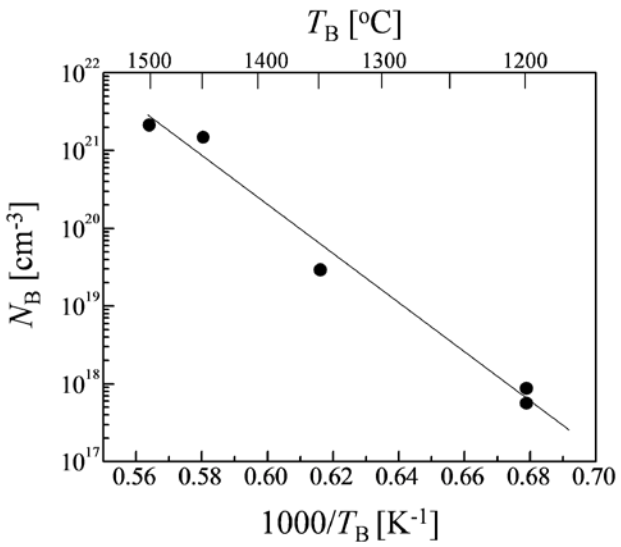

Fig. 1. Arrhenius plot of B concentration N_B.

The X-ray diffraction measurements indicate the *a* axis of $BaSi_2$ crystal grains to be normal to the silicon substrate surface as shown in Fig. 2. The observed (100)-oriented diffraction peaks such as (200), (400), and (600) are seen. Similar *a*-axis-oriented $BaSi_2$ films were obtained for all the samples regardless of B concentration.

Figures 3(*a*) and (*b*) show typical examples of bright-field (BF) and dark-field (DF) TEM images, respectively, along the $BaSi_2$[100] azimuth for undoped $BaSi_2$ on Si (111). The dark-field image was taken under a two-beam diffraction condition to clarify the grain size of $BaSi_2$. The *a*-axis-oriented $BaSi_2$ epitaxial layer has grains with three $BaSi_2$ epitaxial variants rotated by

120 deg to each other in the surface normal direction related to the three fold symmetry of Si(111) [3]. One of them is bright in Fig. 3(*b*). The grain size of undoped $BaSi_2$ films was distributed in the range of 0.2 – 5 μm in the lateral dimensions with the simple orthorhombic crystal structure. The average diameter is approximately 2.7 μm as shown later. The grain size in the MBE-grown $BaSi_2$ is dependent on the RDE growth conditions and can be varied from approximately 0.2 to more than 4 μm on Si(111) [17].

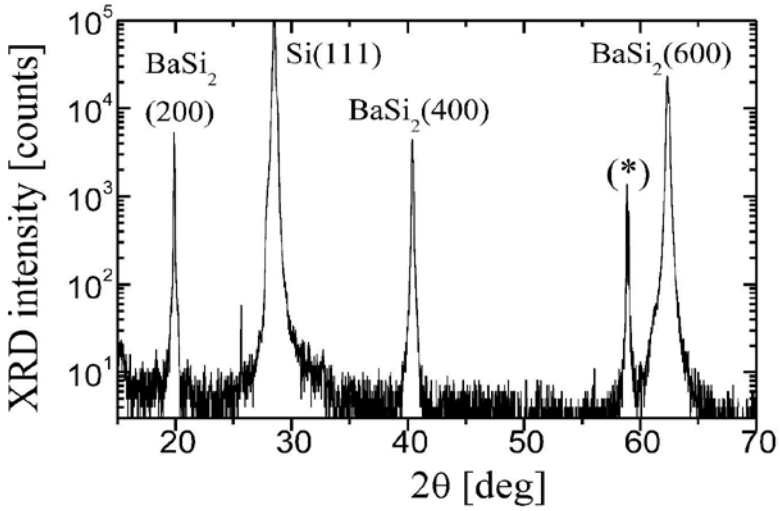

Fig. 2. θ-2θ XRD pattern of $BaSi_2$ film deposited onto monocrystalline Si(111) substrate. The asterisk (*) indicates the peak for the Si substrate.

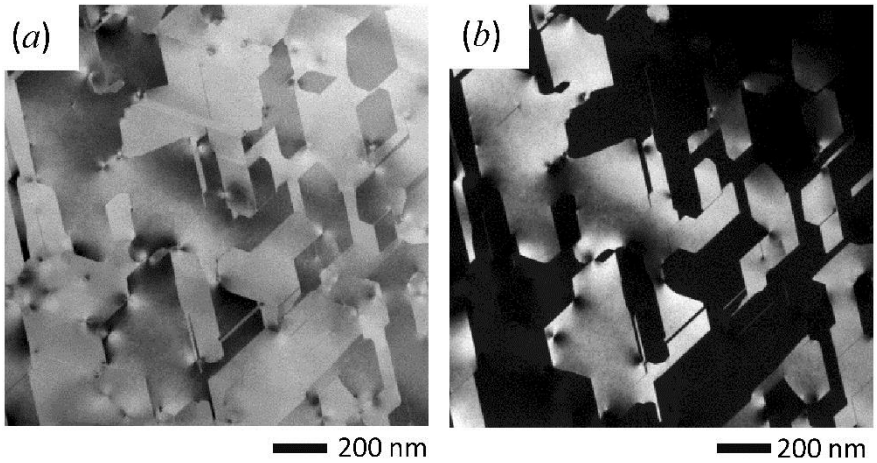

Fig. 3. (*a*) Bright-field and (*b*) dark-field plan-view TEM images of undoped $BaSi_2$ observed along $BaSi_2$ [100]. The incident electron beam was slightly tilted for the grain boundaries to be seen clearly.

Figures 4(*a*) and (*b*) are the counterparts of Figs. 3(*a*) and (*b*), respectively, for B-doped *p*-$BaSi_2$ film grown at T_B=1100 ºC. In comparison with the undoped $BaSi_2$ film in Figs. 3(*a*) and

(*b*), the grain size of B-doped $BaSi_2$ decreased and the grain boundaries became a little dim and roundish, indicating the crystalline quality was degraded with doping. The decrease in the grain size of B-doped $BaSi_2$ is probably attributed to the suppressed migration of Ba and Si atoms during MBE. The dislocations apparently observed in the TEM images of Figs. 3(*a*) and 4(*a*) are characterized by the density of about 3.5×10^9 in undoped $BaSi_2$ and of 5.4×10^9 cm^{-2} in B-doped *p*-$BaSi_2$ at T_B=1100 ºC, indicating that the dislocation concentration increased by the doping of B. These values can be underestimated. Hence, more dislocations are likely to be present in the grown films. With increasing B concentration, B atoms tend to precipitate in $BaSi_2$ [10], and hence those precipitates may act as nuclei for dislocations.

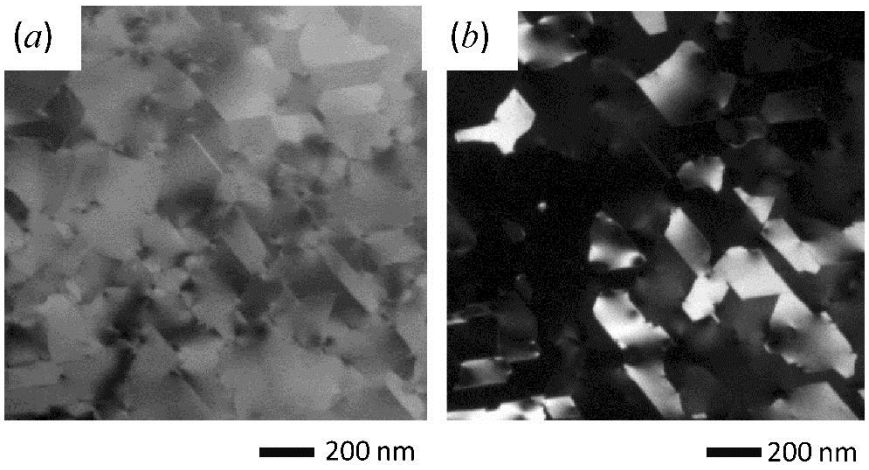

Fig. 4. (*a*) Bright-field and (*b*) dark-field plan-view TEM images of B-doped $BaSi_2$ film with T_B=1100 ºC, observed along $BaSi_2$ [100]. The incident electron beam was slightly tilted for the grain boundaries to be seen clearly.

To provide an overview of how the grain size of $BaSi_2$ film depends on N_B, we have conducted EBSD measurements. Figures 5(*a*) – (*d*) show 12 × 12 μm^2 EBSD crystal orientation maps of $BaSi_2$ epitaxial films on Si(111) and distribution histograms of $BaSi_2$ grain sizes for samples grown at different T_B. Three colors in the orientation maps, that is red, green, and blue, denote three epitaxial variants in the *a*-axis-oriented $BaSi_2$ films. The calculated average sizes of grains are also presented. Although the precise grain size can be obtained by plan-view TEM as presented in Figs. 3 and 4, the EBSD results revealed that the grain size of $BaSi_2$ decreased with

N_B. Completely the same analysis was performed for the undoped and B-doped $BaSi_2$ epitaxial films on Si(001) substrates and the average grain sizes calculated from the histograms was estimated to be 7.8, 5.7 and 4.7 μm for the appropriate samples, respectively. Note that the grain size of $BaSi_2$ films on Si(001) was much larger than that on Si(111), and also decreased when N_B was increased.

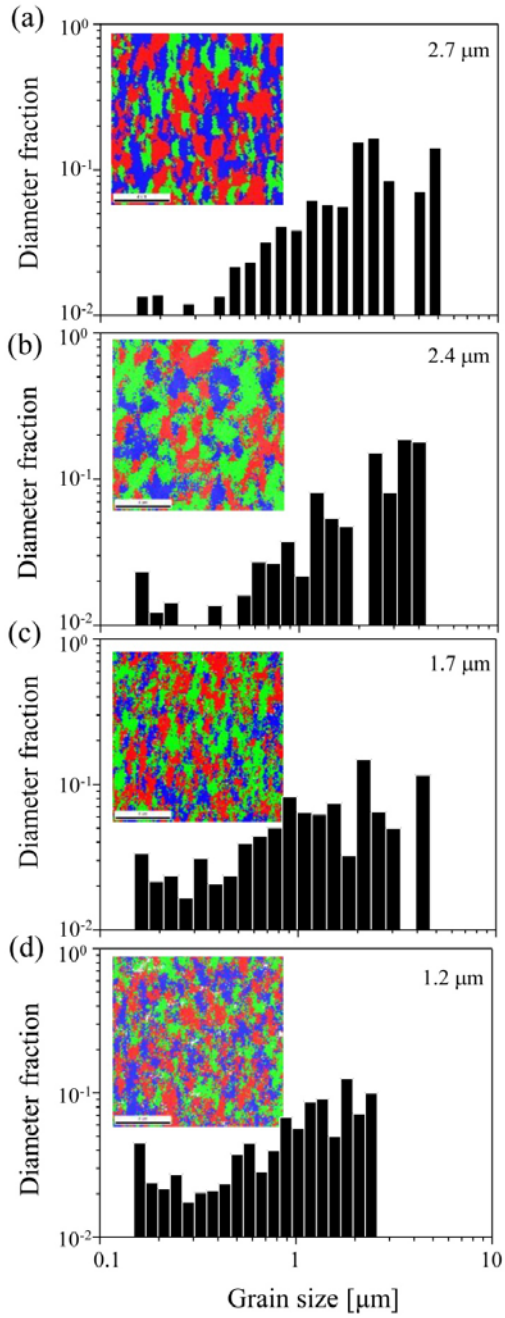

Fig. 5. EBSD crystal orientation maps of $BaSi_2$ epitaxial films on Si(111) and distribution histograms of $BaSi_2$ grain size for samples of grown (*a*) without B (the undoped *n*-$BaSi_2$ sample), with T_B = (*b*) 1000, (*c*) 1170, and (*d*) 1300 ºC. Average grain sizes calculated from the histograms are also presented.

The electron mobility measured as a function of temperature is shown in Fig. 6(*a*) and such a dependence can be conventionally divided into three main regions. The region I ($160 \leq T \leq 218$ K) displays a sharp mobility raise with temperature till it reaches the maximum. The main scattering mechanism here is possibly defined by electron scattering on charge centers since the slope of the mobility curve closely follows the $T^{3/2}$ law [3]. The region II ($218 \leq T \leq 243$ K) represents the region of the mobility maximum, while the region III ($243 \leq T \leq 298$ K) is characterized by the fast mobility drop due to electron scattering on phonons with the almost $T^{-3/2}$ dependence [3]. In addition to that the position of the mobility maximum (1230 $cm^2/V{\cdot}s$ at 218 K) is shifted to the high temperature region as compared to other semiconducting silicides as well as the mobility itself has rather high values [2, 18 – 21]. Meanwhile, the mobility decreases to 816 $cm^2/V{\cdot}s$ at RT.

Hole mobility in B-doped *p*-$BaSi_2$ measured as a function of temperature is shown in Figs. 6 (*b*) and (c). The following features can easily be traced: (1) The mobility (in *p*-$BaSi_2$) at RT is about one order or four times smaller than the electron mobility (in *n*-$BaSi_2$) for the films grown on (111) or (001) Si substrates, respectively. Also the hole mobility at appropriate temperatures has a tendency to decrease considerably from sample to sample when the dopant concentration increases. (2) The effect of scattering on charge centers or at the grain boundaries was traced only at low temperatures (at $T < 100$ K) for the two cases (namely # 4 and 5 in Fig. 6(b)) with the highest dopant concentrations (and also for the smallest average grain sizes). That means such an effect should be noticeable within a more extended temperature range in films with grains smaller than 1 μm. (3) Contrary to *n*-$BaSi_2$ (Fig. 6(*a*)) the mobility maximum is located at temperatures lower than 100 K and for all the cases of *p*-$BaSi_2$ (Figs. 6(*b*) and (*c*)) at $T > 100$ K the charge carrier mobility is defined mainly by scattering on phonons plus possible contribution by scattering on neutral impurity centers (as far the latter to be temperature independent).

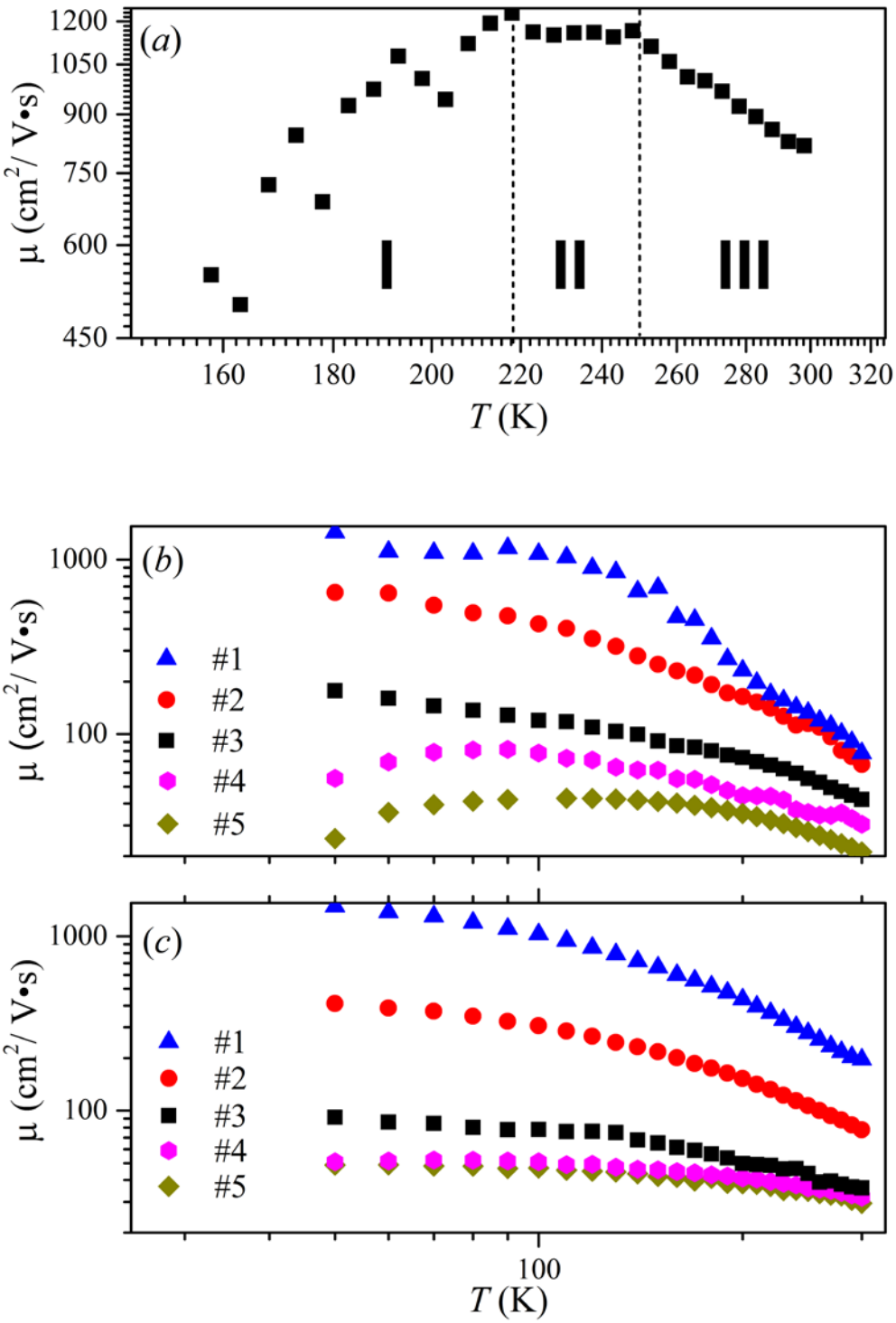

Fig. 6. The experimentally measured carrier mobility versus temperature in $BaSi_2$ films: (*a*) Hall mobility of electrons in undoped films; (*b*) and (c) mobility of holes in p-type films grown on (111) and (001) Si substrates, respectively. The appropriate Hall carrier concentration at RT is shown in brackets after the sample number. The samples have the following values of Hall carrier concentrations (cm^{-3}) at RT: #1 – 4.97×10^{16} ; #2 – 9.39×10^{16} ; #3 – 6.65×10^{17} ; #4 – 4.8×10^{18} ; #5 – 5.26×10^{18} for Si(111) and #1 – 5.5×10^{16} ; #2 – 2.06×10^{17} ; #3 – 1.9×10^{18} ; #4 – 4.57×10^{18} ; #5 – 1.1×10^{19} for Si(001).

3. Simulation

Several standard and well-known scattering mechanisms are usually considered in semiconductors [22, 23]. Each mechanism can be described by the complex function of meaningful physical values which can be treated as an appropriate set of parameters. In our case if one accounts for all the possible scattering mechanisms the resulting mobility according to the Mathiessen's formula is

$$1/\mu = 1/\mu_{AC} + 1/\mu_{NPO} + 1/\mu_{PO} + 1/\mu_{CIC} + 1/\mu_{NIC}, \quad (1)$$

where μ_{AC}, μ_{NPO}, μ_{PO}, μ_{CIC}, μ_{NIC}, are partial mobilities defined by carrier scattering on acoustic phonons, nonpolar and polar optical phonons, and charge and neutral impurity centers, respectively. Previously this approach was used for a number of semiconducting silicides [18 – 21].

In the case of parabolic bands and nondegenerate charge carriers for each separate mechanism one has [22, 23]

$$\mu_i = \frac{4q}{3m^*(kT)^{5/2}\sqrt{\pi}} \int_0^\infty E^{\frac{3}{2}} \tau_i \exp\left(-\frac{E}{kT}\right) dE, \quad (2)$$

where m^* is the carrier effective mass (for electrons in bulk $BaSi_2$ it is 0.42 with m_{xx}=0.6; m_{yy}=0.37; m_{zz}=0.3 and for holes it is 0.57 since m_{xx}=0.31; m_{yy}=0.73; m_{zz}=0.67 in units of free-electron mass [8]), q is the electron charge, T is the absolute temperature, k is the Boltzmann constant, and τ_i is the momentum relaxation time of the i-th mechanism.

For acoustic phonon scattering the relaxation time is [22, 23]

$$\tau_{AC} = \frac{\pi \hbar^4 q^2 \rho v_s^2}{\sqrt{2m^{*3}E}D^2 kT}, \quad (3)$$

where ħ is the reduced Plank constant, ρ is the material density (3.66 g/cm^3 for $BaSi_2$ [2]), v_s is the mean longitudinal sound velocity (4.1×10^5 cm/s for $BaSi_2$ [7]) , and D is a constant defined by the components of the deformation potential tensor. Usually it varies from 5 to 15 eV in semiconductors [22, 23].

For optical nonpolar phonon scattering the relaxation time is [22, 23]

$$\tau_{NPO} = \tau_{AC}\left[C\left(1+\frac{kT_0}{E}\right)^{\frac{1}{2}} + \exp\left(\frac{T_0}{T}\right)\left(1-\frac{kT_0}{E}\right)^{\frac{1}{2}}\right]^{-1}, \quad (4)$$

here $T_0 = \hbar\omega_0/k$, where ω_0 is the optical phonon frequency, $C = \eta/2\left(\frac{T_0}{T}\right)\left(\exp\left(\frac{T_0}{T}\right)-1\right)^{-1}$, and $\eta = (D_{NPO}/D_{AC})^2$. The latter ratio of the nonpolar optical deformation potential to the acoustic one is a parameter of the model.

Recently the thermoelectric properties of $BaSi_2$ were studied as well as the longitudinal sound velocity was experimentally measured and the Debye temperature was estimated to be as low as 260 K for the acoustical mode of the phonon spectrum [7]. On the other hand, the lattice dynamic properties were estimated from the first principal calculations [24] pointing out from the presented phonon band structure that there are several optical modes and the highest frequency of the optical modes is 493 cm^{-1} which corresponds to the Debye temperature to be about 700 K. Moreover it should be noted that for acoustic phonons the Debye temperature has been estimated to be 240 K which correlates well with experimental data [7].

The momentum relaxation time due to polar optical phonon scattering is [22, 21]

$$\tau_{PO} = \sqrt{\frac{2^5 E}{m^*}}\frac{\pi\hbar^2\varepsilon_p}{kT_0 q^2}\left\{n(T_0)\left(1+\frac{kT_0}{E}\right)^{\frac{1}{2}} + [n(T_0)+1]\left(1-\frac{kT_0}{E}\right)^{\frac{1}{2}}\right. \quad (5)$$

$$\left. + \frac{kT_0}{E}\left[(n(T_0)+1)\,\mathrm{arcsinh}\left(\frac{E}{kT_0}-1\right)^{\frac{1}{2}} - n(T_0)\,\mathrm{arcsinh}\left(\frac{E}{kT_0}\right)^{\frac{1}{2}}\right]\right\}^{-1},$$

where $n(\omega_0)=(\exp(\hbar\omega_0/kT)-1)^{-1}$, $\varepsilon_p = (1/\varepsilon_{in} - 1/\varepsilon_0)$, ε_{in} and ε_0 are the high-frequency and the static dielectric constants ($\varepsilon_0 = 14.6$ and $\varepsilon_{in} = 3.2$ for $BaSi_2$ [8]), respectively.

Currently, there are some models describing scattering by charge centers, such as the Brooks–Herring or Conwell–Weisskopf models [22, 23] or recently proposed modified model by N. A. Poklonski *et al.* [25]. However, they all give qualitatively the same results. For the scattering by charge centers the relaxation time is given by [22, 23]

$$\tau_{CIC} = \left[\frac{\pi N_i Z^2 q^4}{\varepsilon_0^2 E^{\frac{3}{2}} \sqrt{2m^*}} \left\{ \ln(1+x) - \frac{x}{1+x} \right\} \right]^{-1}, \quad (6)$$

where N_i is the charge centers concentration, Z is the charge value of the center, $x = 8mEr_0^2/\hbar^2$, $r_0 = (\varepsilon_0 kT/4\pi nq^2)^{1/2}$ is the Debye screening radius, n is the self-carrier concentration ($n = 5.0 \times 10^{15}$ cm^{-3} for $BaSi_2$). And finally the Erginsoy's formula can be used [22, 23] for the neutral impurity scattering mechanism

$$\tau_{NIC} = \left[\frac{20\varepsilon_0 N_0 \hbar^3}{m^{*2} q^2} \right]^{-1}, \quad (7)$$

where N_0 is the neutral center concentration.

Summarizing for the theoretical simulation we accounted for carrier scattering by the different kinds of phonons and by charge and neutral impurity centers. Generally, there are other possible scattering mechanisms [22, 26], but they do not play a noticeable role for our particular cases. As far as the dislocation density was estimated to be of the order of less than 10^{10} cm^{-2} in all our studied samples of $BaSi_2$ and the mentioned mechanism would influence the resulted mobility for the density to be at least of the order of 10^{11} cm^{-2}, we have excluded the carrier scattering by the dislocations from the analysis. Thus, in our theoretical modeling we have only 4 unknown parameters: D (constant defined by the components of the deformation potential tensor), η (ratio of polar optical phonons to acoustic phonons deformation potential tensors) and the charge (N_i) and neutral (N_0) impurity center concentrations as far as we know nothing *a priori* or from the experimental data about their possible values. All the other parameters for the scattering mechanisms considered were experimentally measured or reliably estimated.

3.1 Simulation of the electron mobility in grained $BaSi_2$ films

All the above mentioned mechanisms of electron scattering represented by formulae (3) through (7) were accounted for the numerical simulation of the electron mobility in $BaSi_2$ as a function of temperature. The main results are shown in Fig.7. We have found a lot of reasonable

sets of realistic parameters to reproduce only the region I or III of the experimental curve in addition to a few reasonable sets of realistic parameters to reproduce at least qualitatively *e.g*. the regions II and III of the experimental curve simultaneously as shown in Fig. 7(*a*). The latter results were obtained for the following set of parameters: D = 4 eV; η = 5; $N_i = 2.0 \times 10^{16}$ cm^{-3} and $N_0 = 5.0 \times 10^{15}$ cm^{-3} or less. Also we need to emphasize that the Debye temperature is one of the key parameters to reproduce the experimental data correctly. In our case the Debye temperature of 850 – 900 K is considerably higher than the possible experimental one of 700 K. And finally we stress out that one can correctly reproduce either the mobility rise with temperature due to scattering on charge impurity centers as well as the presence of the mobility maximum (to be about 1230 cm^2/V·s) at the appropriate temperature (at 218 K) or the mobility drop with temperature due to scattering on phonons along with the correct position of the mobility maximum. But there is no any reasonable set of realistic parameters that allows one to reproduce *at the same time* all the regions of the experimental mobility data within the standard theoretical approach. In fact, in the theoretical modeling the region II is always rather broad as clearly seen in Fig. 7(*a*).

It is evident that for an adequate description of the observed experimental data the theoretical approach requires some modifications. We make the following assumptions. The first one is the grained nature of the studied samples. Thus, the intergrain boundaries can be treated as small potential barriers [26] preventing charge carriers to escape from a grain at low temperatures and specific activation energy is necessary to overcome the barrier. And the second assumption takes into consideration the fact that in general experimentally obtained Hall mobility is 1.13…1.98 times larger than the drift one, depending on the scattering mechanism [22, 23]. Thus the resulting mobility can be written as $\mu^* = \gamma \cdot \mu \cdot \exp(-E_{GB}/kT)$, where E_{GB} is the potential barrier height at grain boundaries and γ is the Hall factor. Fig. 7(*b*) represents the results of the simulation by implementing this modified approach with the following set of parameters: D = 4 eV; η = 2; $N_i = 8 \times 10^{15}$ cm^{-3}, $N_0 = 5.0 \times 10^{15}$ cm^{-3} or less and E_{GB} = 62 meV;

γ = 1.8 and 1.2 for scatterings on charge centers and phonons, respectively. Here we note that the obtained value of the barrier height correlates well with the experimentally estimated one of 50 meV [27], while the relative lowering of the Debye temperature results in nonadequate reproducing of the experimental data. However, it is also important to account for scattering on the charge impurity centers even at their relatively low concentrations (N_i of order of 10^{16} cm^{-3}). Moreover, recently it was proposed [28] that Si vacancies in $BaSi_2$ are responsible for the presence of such centers and their estimated concentration is in very good agreement with the results of our study. Such a simple approach allows one to understand the physics of the processes as well as it shows the importance to include the carrier tunneling through the intergrain potential barriers into consideration.

Another possible more strict and rigorous approach is to include directly in Eq. (1) one additional term which describes charge carrier scattering by the grain boundaries [26], namely

$$\mu_{GB} = \frac{qL_D}{\sqrt{8m^*\pi kT}} \exp\left(-\frac{E_{GB}}{kT}\right), \quad (8)$$

where L_D is the average grain size. Practically the same results as presented in Fig. 7(*b*) was reproduced by using this approach with the following set of parameters which summarized in Table 1 (the other parameter values were used as mentioned above) for the structures with three various grain size values. Here we emphasize that the most crucial parameter is the intergrain potential barrier height. The more the average grain size the higher the intergrain barrier. For the structures with large grains the barrier height value could be twice or even more higher than that preliminary estimated from the experiment [27]. Also note that the concentration of the charge centers should be also substantially higher than 10^{16} cm^{-3} which was estimated before [27]. So the adequate values of the intergrain potential barrier height as well as the concentrations and the nature of various point defects in the material need to be investigated more thoroughly both from the experimental and theoretical point of view.

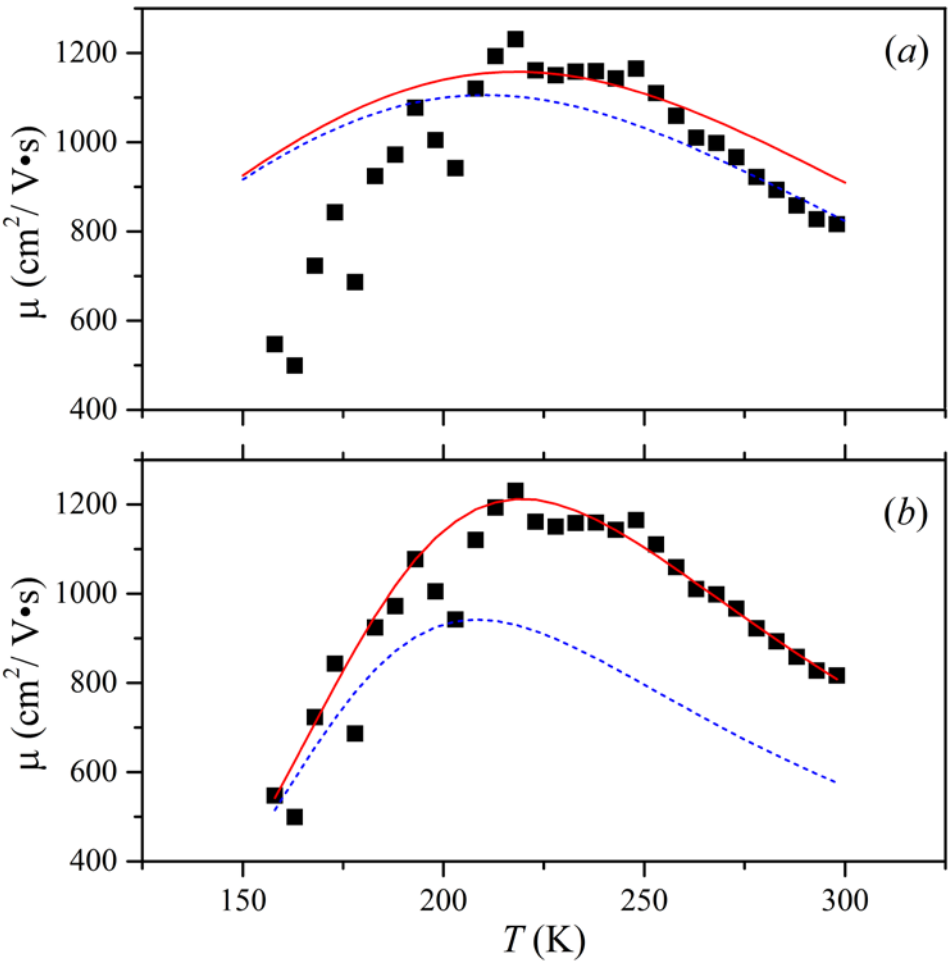

Fig. 7. Electron mobility versus temperature in *n*-$BaSi_2$ films: (*a*) comparison of the experimental data and theoretical results within the standard approach (experiment – black squares, simulation – solid and dashed curves: the upper solid curve at T_0 = 900 K and lower dashed one at T_0 = 850 K); (*b*) comparison of the experimental data and theoretical results within the modified model (experiment – black squares, simulation – solid and dashed curves: the upper solid curve at T_0 = 700 K and the lower dashed one at T_0 = 540 K).

Table 1. Parameters used in the simulation of carrier mobility: D (constant defined by the components of the deformation potential tensor), N_i (charged impurity center concentration), E_{GB} (potential barrier height) and L_D (average grain size).

L_D (μm)	E_{GB} (meV)	N_i (cm^{-3})	D (eV)
0.25	100	9×10^{15}	4
2.5	131	$10 - 12 \times 10^{16}$	3.5
5.0	141	$14 - 15 \times 10^{16}$	3.4

3.2 Simulation of the hole mobility in grained $BaSi_2$ films

We have also performed the theoretical simulation (hole scattering mechanisms represented by Eq. (3) through (8)) of the hole mobility according to the experimental data for B-doped $BaSi_2$ grown on Si(111) and our best theoretical fits are presented in Fig. 8. The data on the parameter values used in calculations are summarized in Table 2. To correctly reproduce the main features in the experimental temperature dependence of the hole mobility one should assume first of all that the *D* parameter value (which is characterized by the strength of the carrier-phonon interaction) is significantly different for the *n*- and *p*-type $BaSi_2$. This is due to the fact that in spite of the effective masses of electrons and holes are of the same order, the energy band extrema for the corresponding carriers are located in different **k**-points of the Brillouine zone (the maximum of the valence band is in the 0.7 × Γ-Y point, the minimum of the conduction band is in the T point [8]). It results in different values of the deformation potential tensors (as shown for some other materials such as Si, Ge, Bi [29]). Thus, the specific features of electron-phonon and hole-phonon coupling are mainly responsible for such a great difference in the corresponding values of electron and hole mobilities.

Then it should be emphasized that the grain effect in mobility properties is negligible for the first three samples (#1-3) with the average grain size of more than 1.5 μm (Fig. 8(*a*)). In this case one should assume the appropriate intergrain potential barrier height to be less than 10 meV. Also it is interesting to note that for an adequate description of low temperatures behavior of hole mobility (at $T < 100$ K) for the rest of the samples (#4-5) with the highest dopant concentration (Fig.8(*b*)) more pronounced potential barrier associated with the grain boundaries should be introduced. Our estimates of the barrier heights to be 45 – 48 meV are consistent with the experimental data. According to [30] the barrier heights at the grain boundaries in *p*-$BaSi_2$ were estimated to be a few tens of meV. Also it should be emphasized here that the value of the intergrain potential barrier is rather different for the electron and the hole subsystems. On the whole it can be treated as an analogous of different band offset for the conduction and valence

bands in heterojunctions. Moreover, there is one more feature for B-doped *p*-$BaSi_2$, namely, scattering on the neutral impurity centers has a great influence on the carrier mobility versus temperature behavior. One could note a strong increase of the concentration of neutral impurity centers with the dopant concentration. We think that this issue can be originated from the formation of a relatively deep donor/acceptor + vacancy level, which is initially in a charged state while after thermal activation it becomes neutral [31]. The same tendency is valid for the charge impurity center concentration. Also it is interesting to note that MBE-grown $BaSi_2$ films can contain rather high concentration of oxygen atoms [32]. In more detail, the possible mechanisms contributing to the Hall concentration, the concentration of neutral and charged centers are considered below.

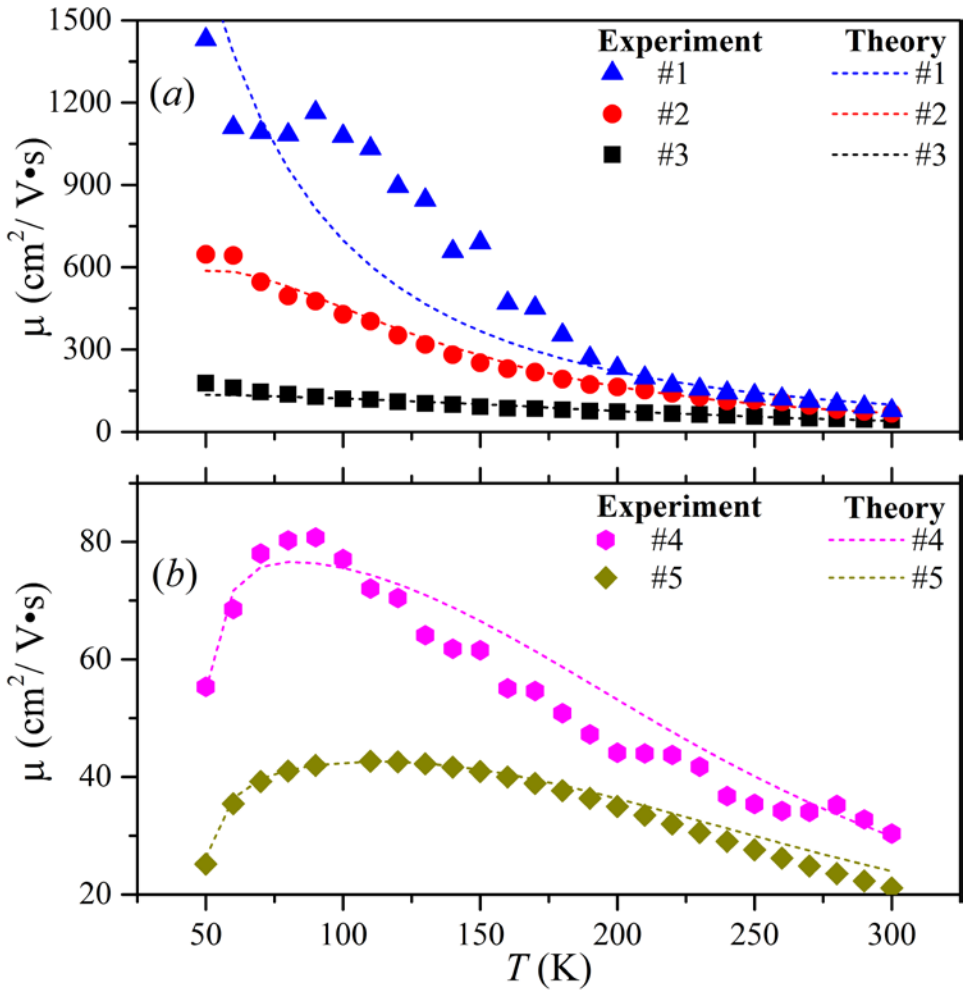

Fig. 8. Hole mobility versus temperature in *p*-$BaSi_2$ films on Si(111): (*a*) comparison of the experimental data and theoretical results for the #1 – #3 samples; (*b*) comparison of the experimental data and theoretical results for the #4 – #5 samples

Table 2. Parameters used in the simulation of carrier mobility: D (constant defined by the components of the deformation potential tensor), η (ratio of polar optical phonons to acoustic phonons deformation potential tensors), the charged (N_i) and neutral (N_0) impurity center concentrations, E_{GB} (potential barrier height) and L_D (average grain size). The appropriate L_D values for the #2 and #4 samples (both on Si(111) and Si(001)) were obtained by the interpolation.

Si(111)						
	N_i (cm^{-3})	N_0 (cm^{-3})	D (eV)	η	E_{GB} (meV)	L_D (μm)
n-type	8×10^{15} or higher	5×10^{15} or less	4	2	62 or higher	0.25 or higher
p-type						
# 1	1×10^{16}	5×10^{16} or less	12.5	1	10 or less	2.4
# 2	4×10^{16}	3.5×10^{17}	12.5	3	10 or less	2.0
# 3	8×10^{16}	3.3×10^{18}	12.5	5	10 or less	1.7
# 4	2×10^{17}	5.5×10^{18}	14	5	45	1.3
# 5	8×10^{17}	9.5×10^{18}	14	5	48	1.2
Si(001)						
p-type						
# 1	3×10^{16}	5×10^{16}	9	1	10 or less	7.8
# 2	7×10^{16}	7.2×10^{17}	12	3		6
# 3	7×10^{16}	6×10^{18}	12.5	3		5.7
# 4	2×10^{17}	9×10^{18}	12.5	3		5.2
# 5	2×10^{17}	1×10^{19}	12.5	3		4.7

One should note that unlike the situation with n-type or p-type $BaSi_2$ on Si(111) substrate the grain effect in mobility properties of the samples grown on Si(001) substrates is negligible for all the samples (#1-5) in this case. This is due to the fact that, on the one hand, here we deal

with the structures that consist of much larger grains and, on the other hand, it seems the appropriate intergrain potential barrier height to be less than 10 meV for such of the grains. All the above mentioned mechanisms of hole scattering represented by formulae (3) through (7) were accounted for in the numerical simulation of the hole mobility in $BaSi_2$ as a function of temperature. The main results are shown in Fig. 9. The data on the parameter values used in calculations are summarized in Table 2. On the whole, the experimental results show the mobility values for the samples with low dopant concentration to be noticeably higher in our case as compared to ones obtained for the films fabricated on Si(111) substrates. From our point of view this fact could be connected first of all with the significant difference in the sizes of the grains in the polycrystalline films generated on different Si substrates. And as a consequence this leads to the changes in the values of deformation potential which characterize the intense of the phonon-hole interaction. Thus we can suggest that there is some weak D and η dependence on the reciprocal effective grain size. Generally the same tendency was observed for the *p*-doped $BaSi_2$ samples on Si(111) substrates as well. Unfortunately, any theoretical quantitative estimates of this function *a priori* could not be done. Moreover any precise empirical attempt to establish such the function is also problematic due to the fact that the grain size distribution in our cases have a non-central character, *i.e.* a whole ensemble of the grains with rather close but different sizes almost equally make contributions to the resulting value of the mobility.

Like the situation with the B-doped *p*-$BaSi_2$ films on Si(111) substrates there is one more feature for the films on Si(001) substrates, namely, scattering on the neutral impurity centers has a great influence on the carrier mobility versus temperature behavior. One could note in Table 2 a strong increase of the concentration of neutral impurity centers with the dopant concentration (not only non-activated boron atoms contribute to the values but it is known that MBE-grown $BaSi_2$ films can contain rather high concentration of oxygen atoms [32]). Also such the trend can be noticed for the concentration of ionized impurity centers. It is interesting to trace how these values are related to the Hall carrier concentration (Fig. 10(*a*)). As seen, the charged center

concentration is significantly less than the Hall carrier concentration whereas the neutral impurity center concentration has higher values as compared with the last one. Moreover the same tendency can be traced for the samples obtained on Si(111) substrates (Fig. 10(*b*)). Accounting for this discrepancy of the values one can conclude there are some other hole activation mechanisms in this compound as compared with the traditional boron activation in silicon. It is known that in complex semiconducting compounds with mixed chemical bonding there are carrier activation mechanisms connected with different lattice defects, deep levels, stoichiometry disorder etc. [26]. Thus, the additional hole concentration in the systems under consideration can be defined by the following possible reasons: (1) if there are interstitial boron and/or oxygen atoms in $BaSi_2$ grains and they provide the additional impurity energy levels which are located not far from the top of the valence band [33]; (2) if there are silicon vacancies in $BaSi_2$ grains (*e.g.* it is a common situation for silicon and germanium where such the defects can be treated as acceptor centers); (3) it is interesting to note that the so-called E-centers (boron + vacancy) and A-centers (oxygen + vacancy) can be treated as the accepter centers as well [31, 33]. Moreover after the thermal activation (annealing) such the centers become neutral. But one need to emphasize that to clarify this issue in details the additional experimental and theoretical investigations should be performed.

Comparison of the data on boron concentration from the SIMS analysis to the data on the charge impurity centers and the Hall carrier concentrations (Fig. 10(*b*)) for the samples #2 – #4 indicates two issues. First of all, it is evident that not all the boron atoms are activated in traditional sense of a word and, secondly, there are some additional mechanisms of carrier activation which should be involved to reproduce the general tendency of the Hall carrier concentration increase. For the extremely low value of boron concentration (4.4×10^{14} cm^{-3}, the sample #1) the role of other point defects or defect complexes in $BaSi_2$ for the carrier activation is crucial. For the highest value of boron concentration (2.1×10^{19} cm^{-3}, the sample #5) it seems the effects of significant boron precipitations occur. Moreover, accounting for high oxygen

concentration in the material under consideration [32] the questions connected with preferable oxygen atom distribution (*e.g.* oxygen precipitations along the intergrain boundaries) also should be studied more in details.

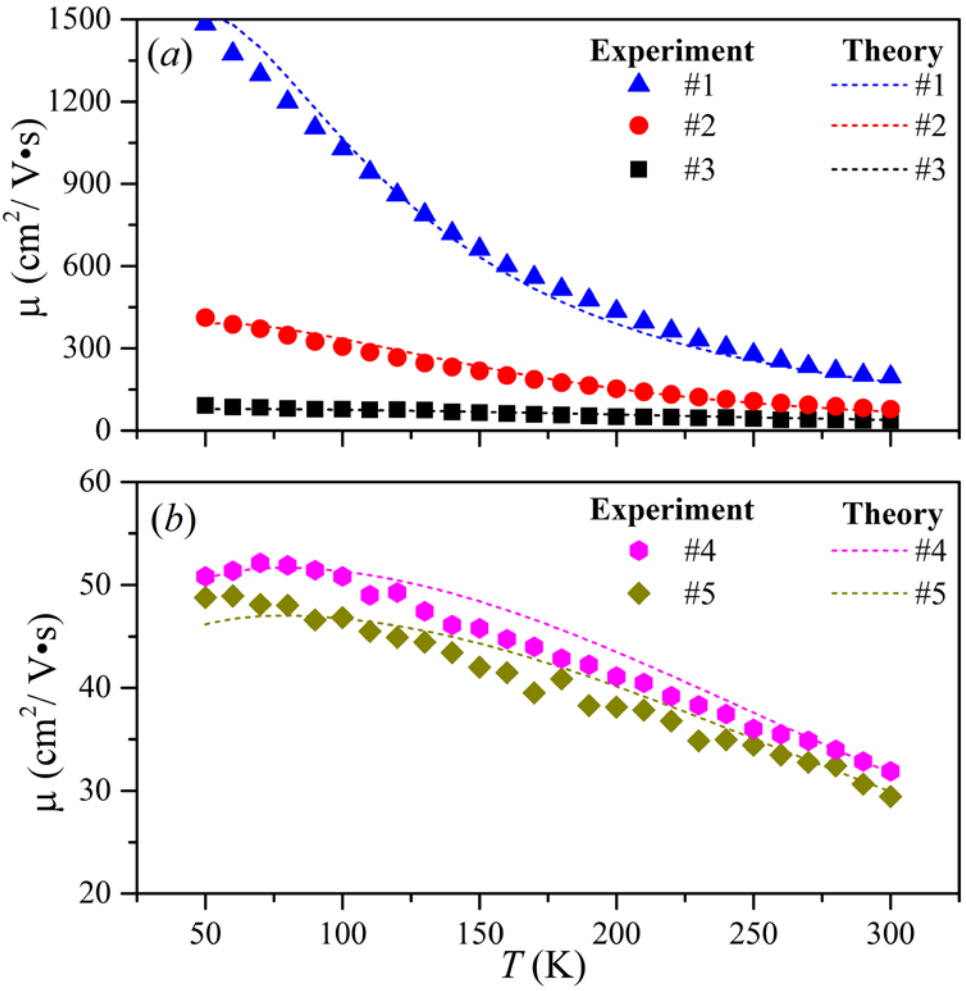

Fig. 9. Hole mobility versus temperature in *p*-$BaSi_2$ films on Si(001): (*a*) comparison of the experimental data and theoretical results for the #1 – #3 samples; (*b*) comparison of the experimental data and theoretical results for the #4 – #5 samples

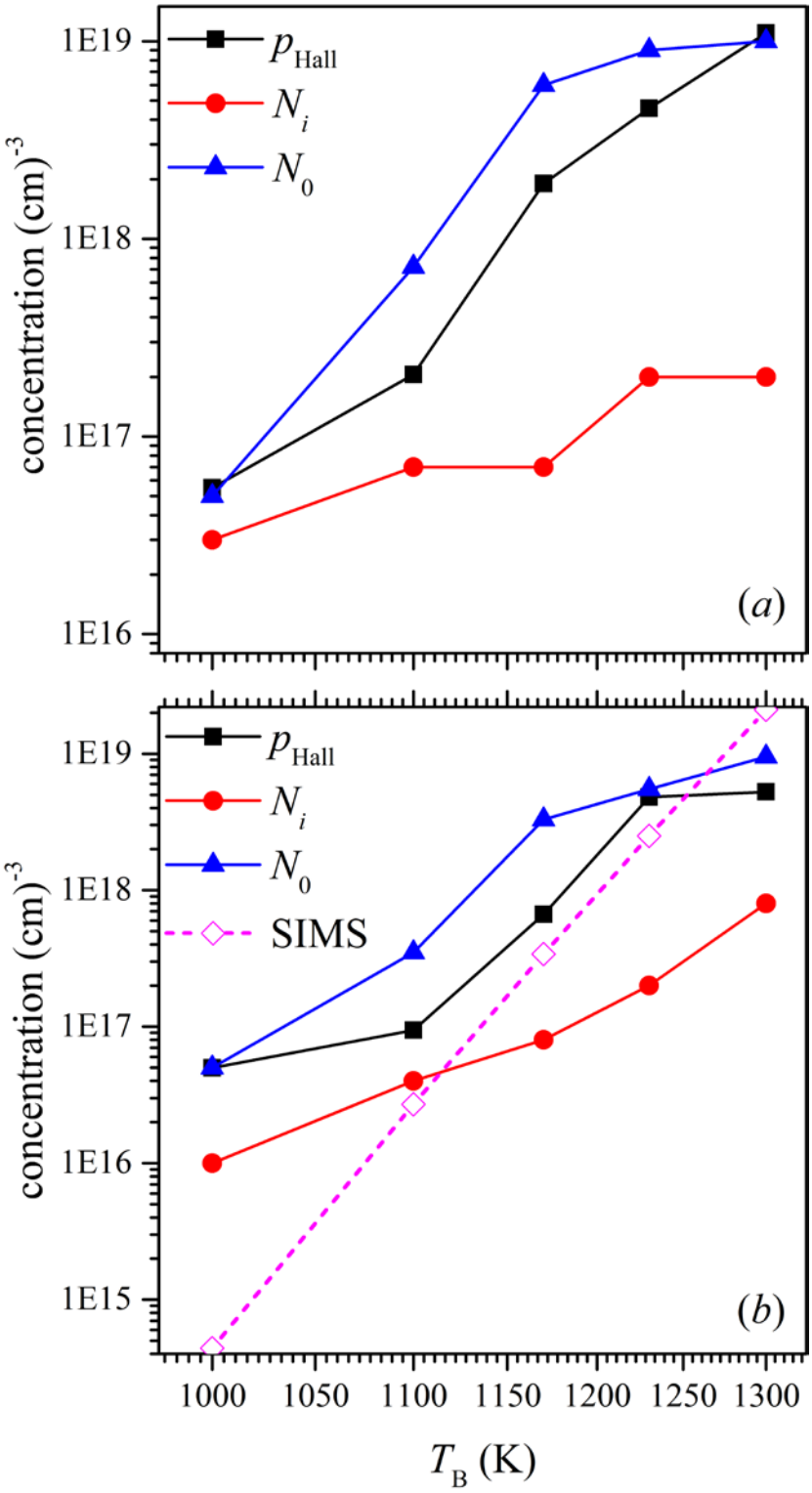

Fig. 10. Experimental Hall carrier concentration (p_{Hall}) for different samples of *p*-$BaSi_2$ films on (*a*) – Si(001) and (*b*) – Si(111) at RT and theoretically estimated both neutral (N_0) and charged (N_i) impurity center concentrations. SIMS data on boron concentration are indicated by the dashed line. T_B are the following: #1 – 1000 ˚C, #2 – 1100 ˚C, #3 – 1170 ˚C, #4 – 1230 ˚C, #5 – 1300 ˚C.

Conclusions

The performed analysis of the experimental temperature dependence of the electron mobility in the grained polycrystalline $BaSi_2$ films with very low impurity concentrations (~ 5.0×10^{15} cm^{-3}) shows that the low temperature part *i.e.* the sharp raise of the mobility (the region I in Fig. 6(*a*)) is mainly defined by intergrain boundaries (~ 60 meV or up to twice higher) to be surpassed by the electrons. The delicate balance between intergrain boundary scattering and scattering on the phonons, the latter defines the high temperature part (the region III in Fig. 6(*a*)), results in the narrow electron mobility maximum (the region II in Fig. 6(*a*)) shifted to higher temperatures as compared with the case of monocrystalline $BaSi_2$ (which is associated with the traditional mechanisms), when intergrain boundaries are absent and scattering at low temperatures is solely defined by charge centers (Fig. 7). To this end, the electron mobility in polycrystalline $BaSi_2$ at 300 K (to be 816 $cm^2/V{\cdot}s$) is larger than in the other semiconducting silicides. The analysis of the experimental temperature dependence of the mobility in the $BaSi_2$ films shows that the hole mobility in *p*-$BaSi_2$ at RT is about one order or four times smaller (depending on the Si substrate) with respect to the electron mobility in *n*-$BaSi_2$. Also the hole mobility values have a tendency to considerably decrease from sample to sample with increasing the dopant concentration. Such a great difference in the corresponding values of electron and hole mobility is primarily due to the specific features of electron-phonon and hole-phonon coupling. On the whole, the hole mobility versus temperature behavior is mainly defined by scattering on phonons and partly by scattering on neutral impurity centers. For device applications, where higher hole mobility values are desirable, we can suggest using $BaSi_2$ grown on Si(100) substrates rather than Si(111) ones.

Acknowledgements

We thank Professor N. A. Poklonski and Dr. N. N. Dorozhkin for the fruitful discussion and useful suggestions on the results of the paper, Dr. N. Yoshizawa and Mr. N. Saito of the National

Institute of Advanced Industrial Science and Technology their TEM observations, and Professor N. Usami of Nagoya University and Dr. K. O. Hara of the University of Yamanashi University for EBSD measurements. This work was financially supported by the Belarusian National Research Programs “Convergence 2020”, “Materials science, new materials and technology”, Belarusian Republican Foundation for Fundamental Research under (Grant No. F18MC-012), the Japan Science and Technology Agency (JST-CREST) and by a Grant-in-Aid for Scientific Research A (15H02237) from the Japan Society for the Promotion of Science (JSPS).

References

[1] T. Dittrich, Materials Concept for Solar Cells, Imperial College Press, 2015.

[2] V.E. Borisenko, Semiconducting silicildes, (Springer Series in MATERIALS SCIENCE, 2000).

[3] T. Suemasu and N. Usami, Exploring the potential of semiconducting $BaSi_2$ for thin-film solar cell applications, J. Phys. D: Appl. Phys. 50 (2017) 023001.

[4] S. Yachi, R. Takabe, H. Takeuchi, K. Toko, T. Suemasu, Effect of amorphous Si capping layer on the hole transport properties of $BaSi_2$ and improved conversion efficiency approaching 10% in p-$BaSi_2$/n-Si solar cells. *Appl. Phys. Lett.* 109 (2016) 072103.

[5] T. Deng, T. Sato, Z. Xu, R. Takabe, S. Yachi, Y. Yamashita, K. Toko, and T. Suemasu, p-$BaSi_2$/n-Si heterojunction solar cells on Si(001) with conversion efficiency approaching 10%: comparison with Si(111), Appl. Phys. Express 11 (2018) 062301.

[6] K. Kodama, R. Takabe, T. Deng, K. Toko, T. Suemasu, Spectroscopic evidence of photogenerated carrier separation by built-in electric field in Sb-doped n-$BaSi_2$/B-doped p-$BaSi_2$ homojunction diodes, Jpn. J. Appl. Phys. 57 (2018) 050310.

[7] K. Hashimoto, K Kurosaki, Y. Imamura, H. Muta, S. Yamanaka, Thermoelectric properties of $BaSi_2$, $SrSi_2$, and LaSi, J. Appl. Phys. 102 (2007) 063703.

[8] D. B. Migas, V. L. Shaposhnikov, V. E. Borisenko, Isostructural $BaSi_2$, $BaGe_2$ and $SrGe_2$: electronic and optical properties, phys. stat. sol. (b) 244 (2007) 2611-2618.

[9] D. B. Migas, V. O. Bogorodz, A. V. Krivosheeva, V. L. Shaposhnikov, A. B. Filonov, and V. E. Borisenko, Electronic properties of thin $BaSi_2$ films with different orientations, Jpn. J. Appl. Phys. 56 (2017) 05DA03.

[10] M. Ajmal Khan, K. Nakamura, W. Du, K. Toko, N. Usami, T. Suemasu, Precipitation control and activation enhancement in boron-doped p^+-$BaSi_2$ films grown by molecular beam epitaxy, Appl. Phys. Lett. 104 (2014) 252104.

[11] D. Tsukahara, S. Yachi, H. Takeuchi, R. Takabe, W. Du, M. Baba, Y. Li, K. Toko, N. Usami, T. Suemasu, p-$BaSi_2$/n-Si heterojunction solar cells with conversion efficiency reaching 9.0%, Appl. Phys. Lett. 108 (2016) 152101.

[12] Y. Inomata, T. Nakamura, T. Suemasu, F. Hasegawa, Epitaxial growth of semiconducting $BaSi_2$ thin films on Si(111) substrates by reactive deposition epitaxy, Jpn. J. Appl. Phys. 43 (2004) 4155-4156.

[13] Y. Inomata, T. Nakamura, T. Suemasu, F. Hasegawa, Epitaxial growth of semiconducting $BaSi_2$ films on Si(111) substrates by molecular beam epitaxy, Jpn. J. Appl. Phys. 43 (2004) L478- L481.

[14] K. Morita, Y. Inomata, T. Suemasu, Optical and electrical properties of semiconducting $BaSi_2$ thin films on Si substrates grown by molecular beam epitaxy, Thin Solid Films 508 (2006) 363-366.

[15] W. Du, M. Baba, K. Toko, K. O. Hara, K. Watanabe, T. Sekiguchi, N. Usami, T. Suemasu, Analysis of the electrical properties of Cr/n-$BaSi_2$ Schottky junction and n-$BaSi_2$/p-Si heterojunction diodes for solar cell applications, J. Appl. Phys. 115 (2014) 223701.

[16] Y. Matsumoto, D. Tsukada, R. Sasaki, M. Takeishi, T. Saito, T. Suemasu, N. Usami, M. Sasase, Epitaxial growth and photoresponse properties of $BaSi_2$ layers toward Si-based high-efficiency solar cells, Jpn. J. Appl. Phys. 49 (2010) 04DP05.

[17] M. Baba, K. Nakamura, W. Du, M. Ajmal Khan, S. Koike, K. Toko, N. Usami, N. Saito, N. Yoshizawa, and T. Suemasu, Molecular Beam Epitaxy of $BaSi_2$ Films with Grain Size over 4 μm on Si(111), Jpn. J. Appl. Phys. 51 (2012) 098003.

[18] D. B. Migas, V. L. Shaposhnikov, A. B. Filonov, V. E. Borisenko, N. N. Dorozhkin, *Ab initio* study of the band structures of different phases of higher manganese silicides, Phys. Rev. B 77 (2008) 075205.

[19] A. B. Filonov, I. E. Tralle, D. B. Migas, V. L. Shaposhnikov, V. E. Borisenko, Transport property simulation of p-type β-$FeSi_2$, phys. stat. sol. (b) 203 (1997) 183-187.

[20] A. E. Krivosheev, L. I. Ivanenko, A. B. Filonov, V. L. Shaposhnikov, G. Behr, J. Schumann, V. E. Borisenko, Thermoelectric efficiency of single crystal semiconducting ruthenium silicide, Semiconductors 40 (2006) 27-32.

[21] A. B. Filonov, A. E. Krivosheev, L. I. Ivanenko, G. Behr, J. Schumann, D. Souptel, V. E. Borisenko, The transport and thermoelectric properties of semiconducting rhenium silicide, Semiconductors 39 (2005) 395-399.

[22] B.K. Ridley, Quantum Processes in Semiconductors, Clarendon Press, Oxford, 1982.

[23] V.L. Bonch-Bruevich, S.G. Kalashnikov, Physics of Semiconductors, Nauka, Moscow, 1990 (in Russian).

[24] H. Peng, C.L. Wang, J.C. Li, R.Z. Zhang, M.X. Wang, H.C. Wang, Y. Sun, M. Sheng, Lattice dynamic properties of $BaSi_2$ and $BaGe_2$ from first principle calculations, Phys. Lett. A 374 (2010) 3797 – 3800.

[25] N.A. Poklonski, S.A. Vyrko, V.I. Yatskevich and A.A. Kocherzhenko, A semiclassical approach to Coulomb scattering of conduction electrons on ionized impurities in nondegenerate semiconductors, J. Appl. Phys. 93 (2003) 9749-9752.

[26] M. Grundmann, The Physics of Semicoductors, 2nd ed. Springer, 2010.

[27] M. Baba, S. Tsurekawa, K. Watanabe, W. Du, K. Toko, K. O. Hara, N. Usami, T. Sekiguchi, T. Suemasu, Evaluation of potential variations around grain boundaries in $BaSi_2$ epitaxial films by Kelvin probe force microscopy, Appl. Phys. Lett. 103 (2013) 142113.

[28] M. Kumar, N. Umezawa, W. Zou, and M. Imai, Barium disilicide as a promising thin-film photovoltaic absorber: structural, electronic, and defect properties, J. Mater. Chem. A 5 (2017) 25293-25302.

[29] V. F. Gantmakher and Y. B. Levinson, Carrier Scattering in Metals and Semiconductors, North Holland, New York, 1987.

[30] D. Tsukahara, M. Baba, S. Honda, Y. Imai, K. O. Hara, N. Usami, K. Toko, J. H. Werner, T. Suemasu, Potential variations around grain boundaries in impurity-doped $BaSi_2$ epitaxial films evaluated by Kelvin probe force microscopy, J. Appl. Phys. 116 (2014) 123709.

[31] Radiation effects in semiconductors, ed. by K. Iniewski. (Boca Raton: CRC Press, 2011).

[32] W. Du, R. Takabe, S. Yachi, K. Toko, T. Suemasu, Enhanced spectral response of semiconducting $BaSi_2$ films by oxygen incorporation, Thin Solid Films 629 (2017) 17-21.

[33] H.F. Matare, Defect electronics in semiconductors, Wiley-Interscience, New York, 1971